

Supporting Information

Carbazole Based Self-Assembled Monolayer as Hole Transport Layer for Efficient and stable $\text{Cs}_{0.25}\text{FA}_{0.75}\text{Sn}_{0.5}\text{Pb}_{0.5}\text{I}_3$ Solar Cells

*Matteo Pitaro, Javier Sebastian Alonso, Lorenzo Di Mario, David G. Romero, Karolina Tran, Teodor Zaharia, Malin B. Johansson, Erik M. J. Johansson, and Maria Antonietta Loi**

M. Pitaro, J. S. Alonso, Dr. L. Di Mario, D.G. Romero, K. Tran, Dr. T. Zaharia, Prof. Dr. M.A. Loi

Photophysics and OptoElectronics

Zernike Institute for Advanced Materials

University of Groningen

Nijenborgh 4, 9747 AG Groningen, The Netherlands

E-mail: m.a.loi@rug.nl

M. B. Johansson, E. M. J. Johansson

Department of Chemistry - Ångström Laboratory, Physical Chemistry

Uppsala University

Lägerhyddsvägen 1 75120 Uppsala, Sweden

Supporting Figures

(a)

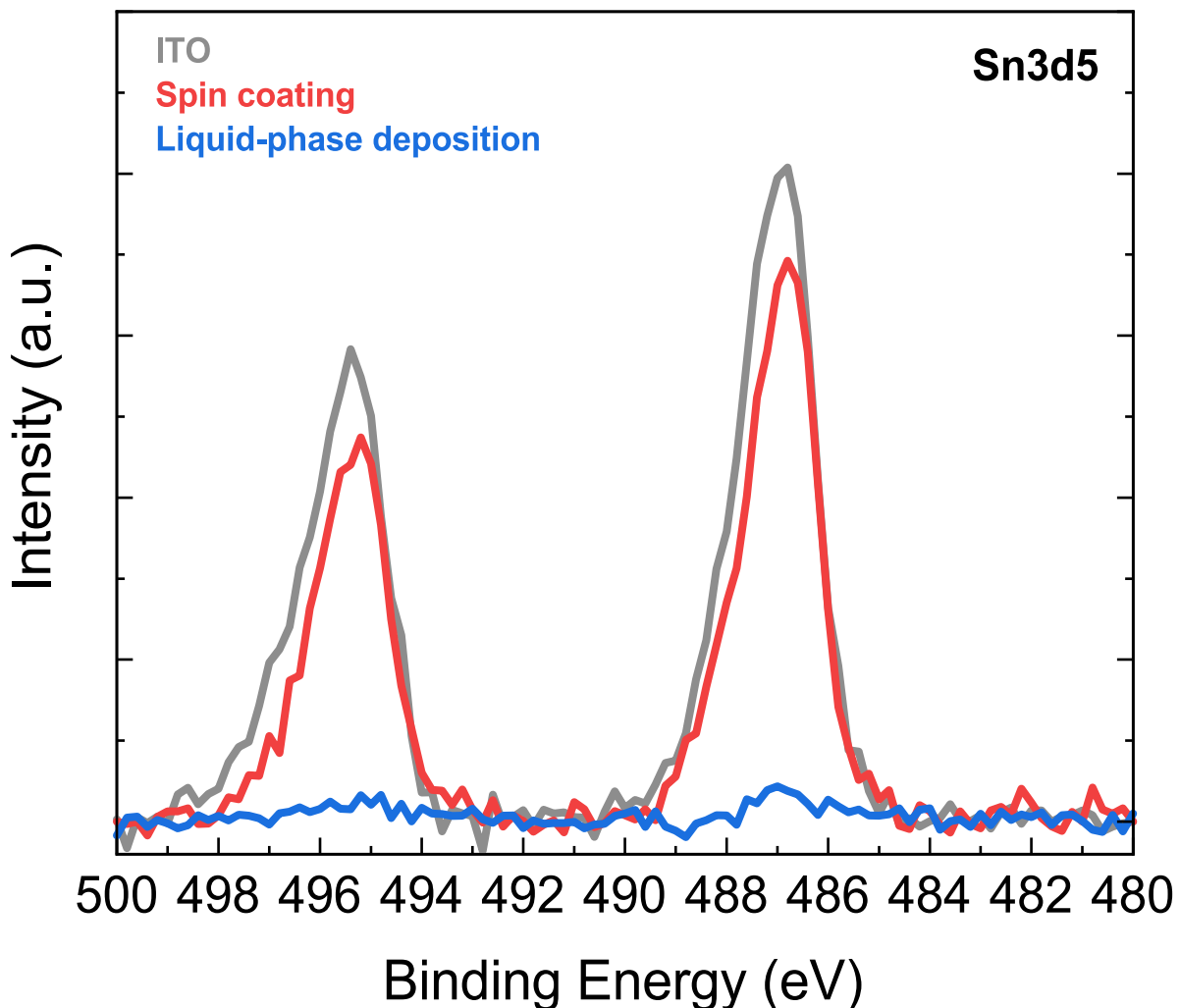


Figure S1. a) Sn3d X-ray photoelectron spectra for ITO (gray line), spin coated SAM (red line), and SAM deposited via liquid-phase deposition (blue line).

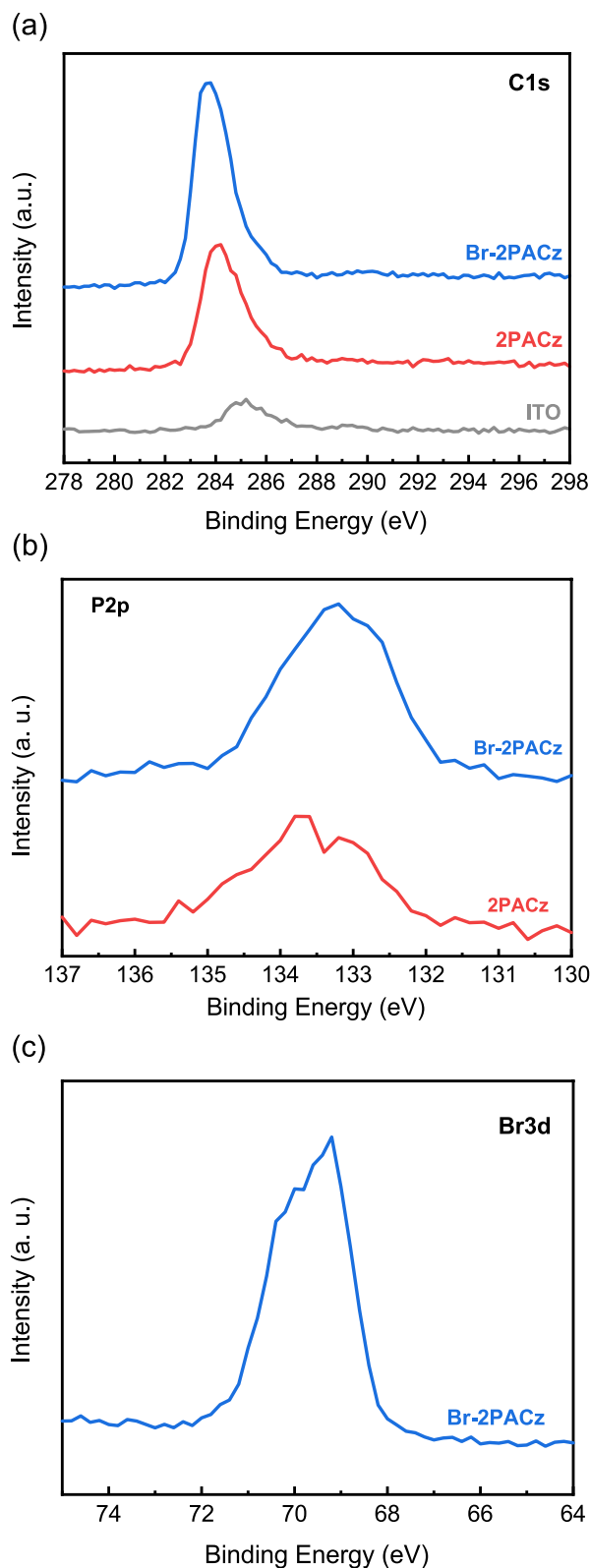
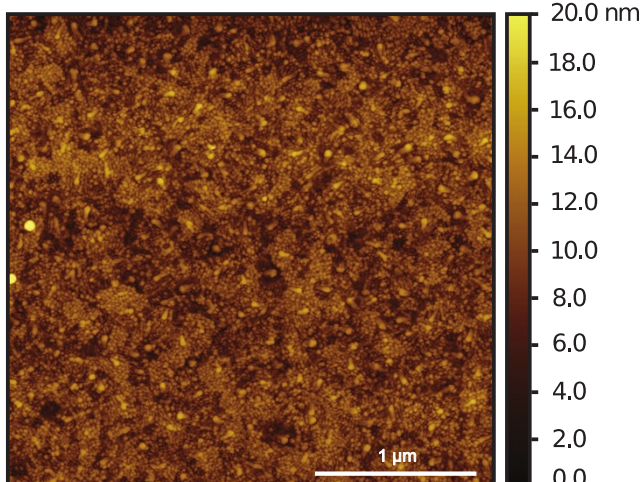
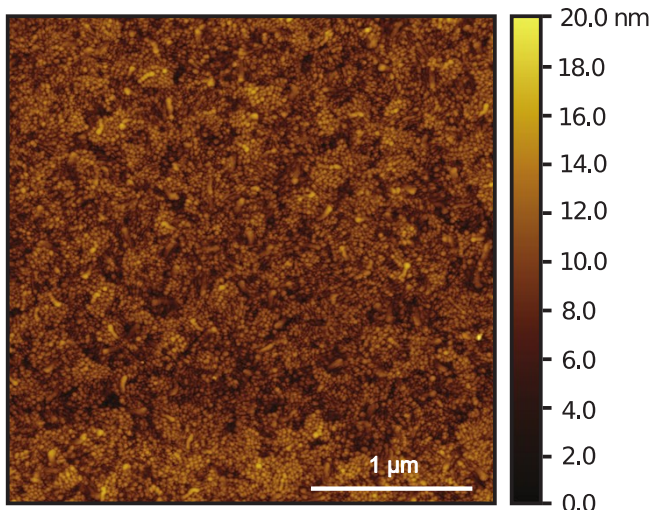


Figure S2. XPS spectra recorded for a) C 1s, b) P 2p, and c) Br 3d regions on ITO (gray line), ITO/2PACz (spin coated, red line), and ITO/Br-2PACz substrates (liquid-phase deposition, blue line).

(a)



(b)



(c)

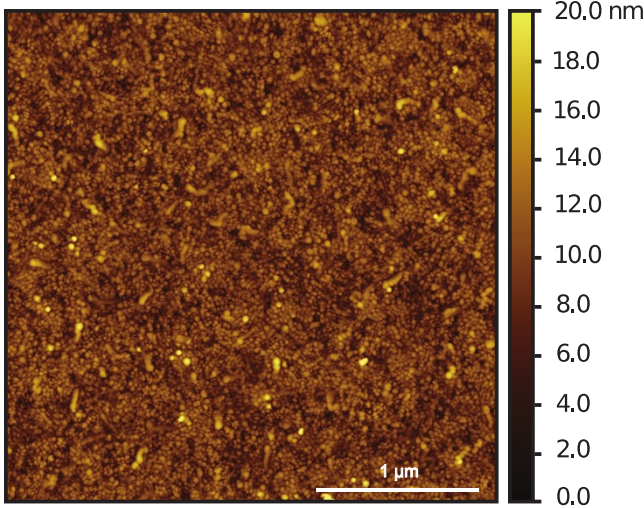
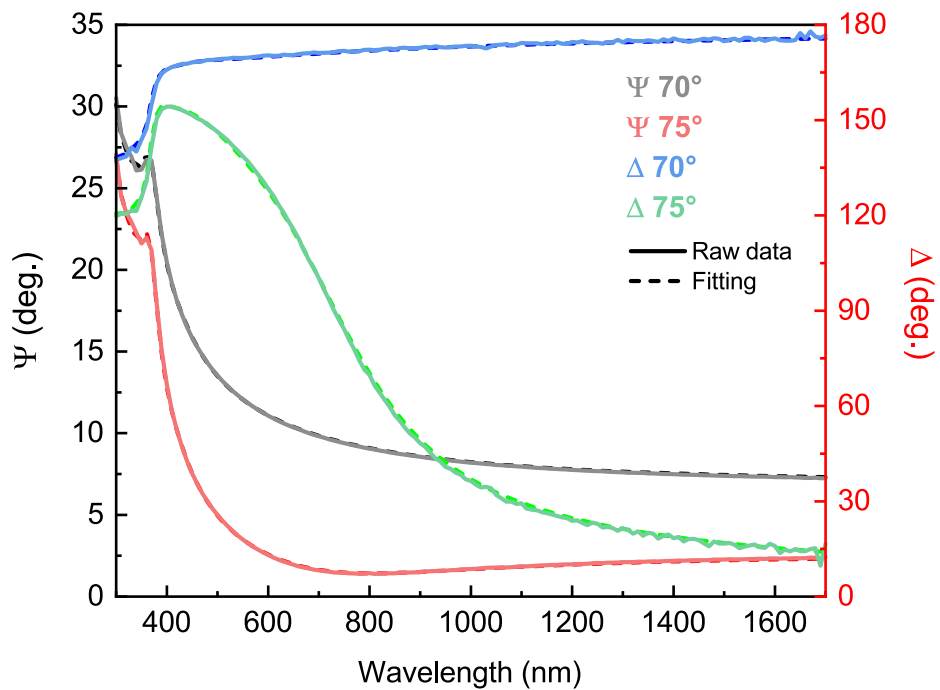


Figure S3. AFM images recorded on a) ITO, b) ITO/2PACz, and c) ITO/Br-2PACz substrates. All the SAMs used for the AFM measurements were deposited by liquid-phase deposition method.

(a)



(b)

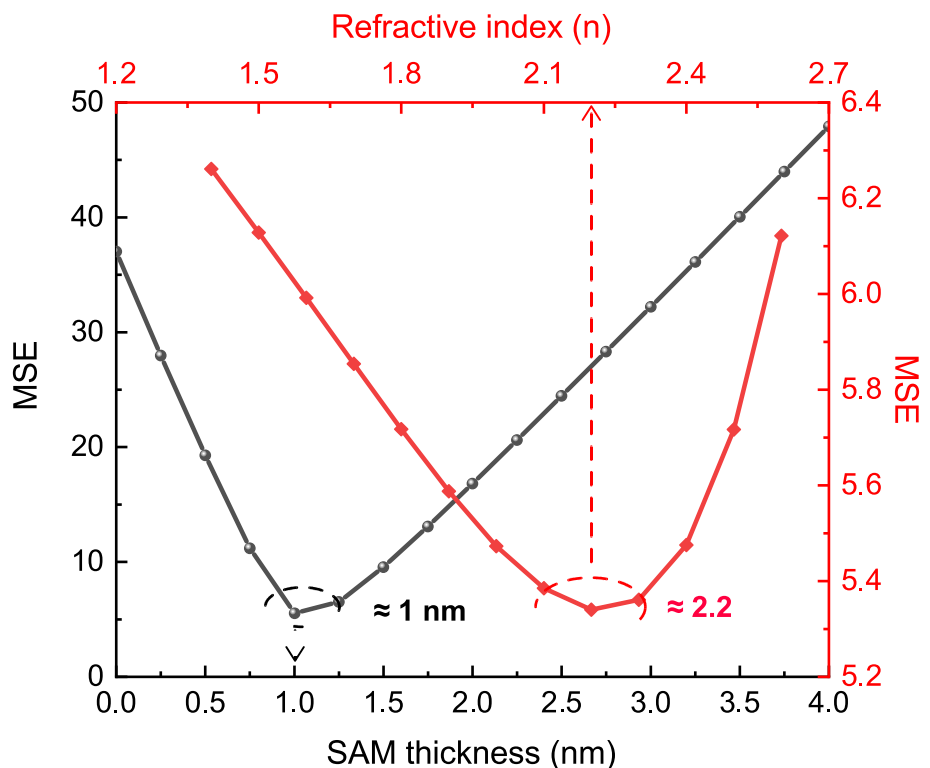


Figure S4. a) Experimental and fitting data of variable angle spectroscopic ellipsometry measurements. Black and red curves shows the Psi values for SiO_x/Br-2PACz samples, while the blue and green curves represents the Delta values for SiO_x/Br-2PACz samples. The measured angles are the 70° and 75°. (b) The Mean Squared Error (MSE) values for different SAM thickness (black curves) and different refractive index values (red curves).

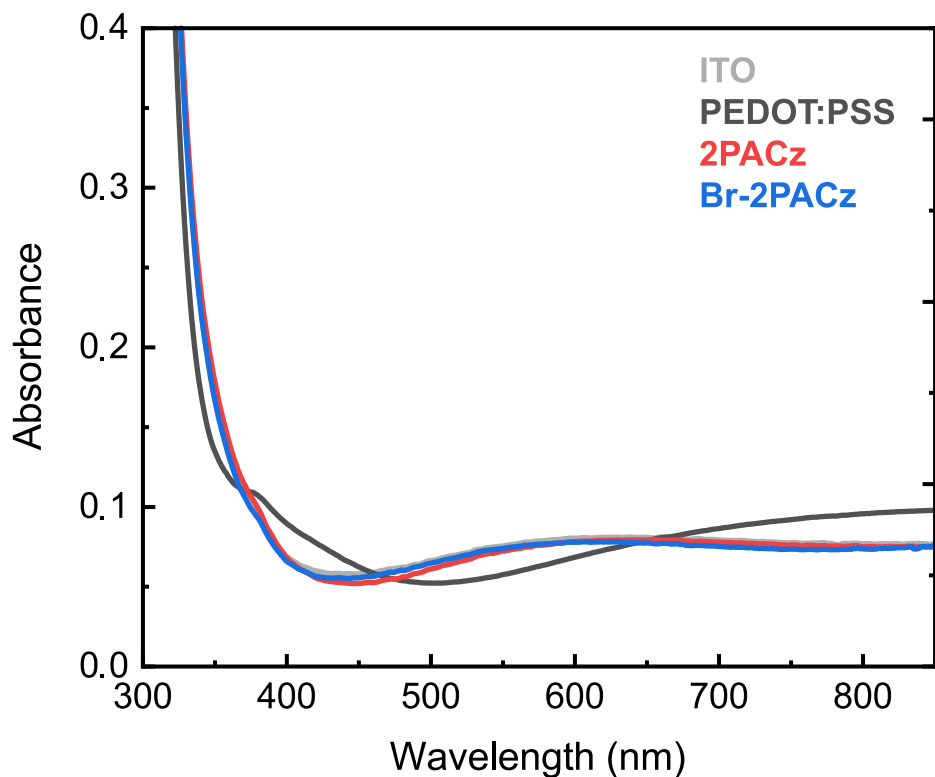
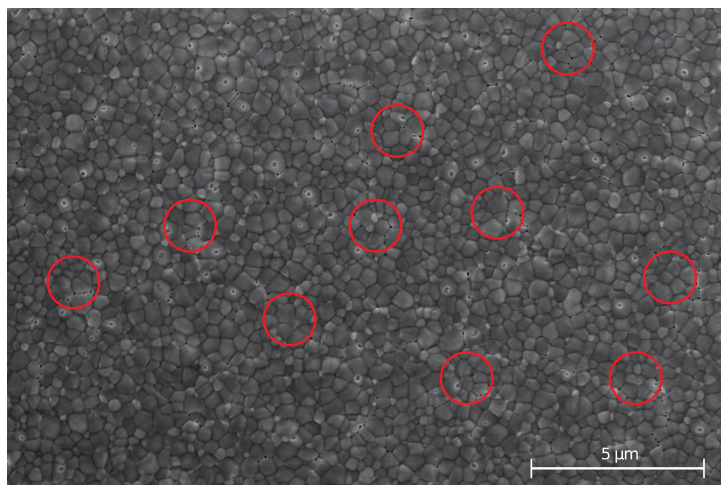
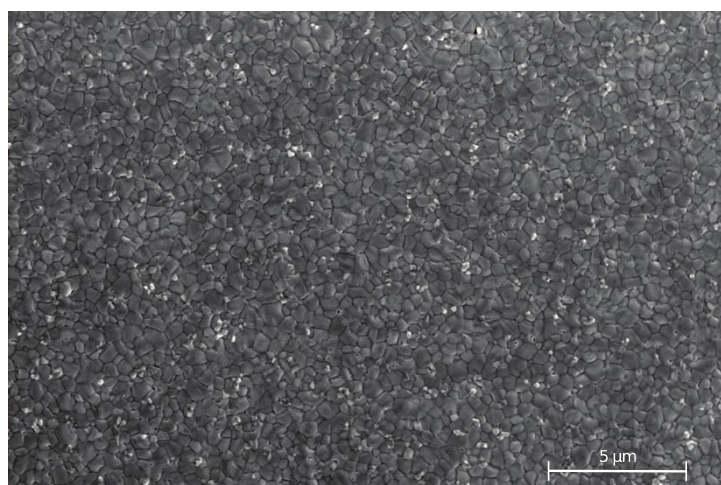


Figure S5. Absorbance spectra of PEDOT: PSS, 2PACz, and Br-2PACz coated on ITO compared to the ITO absorption spectrum.

(a)



(b)



(c)

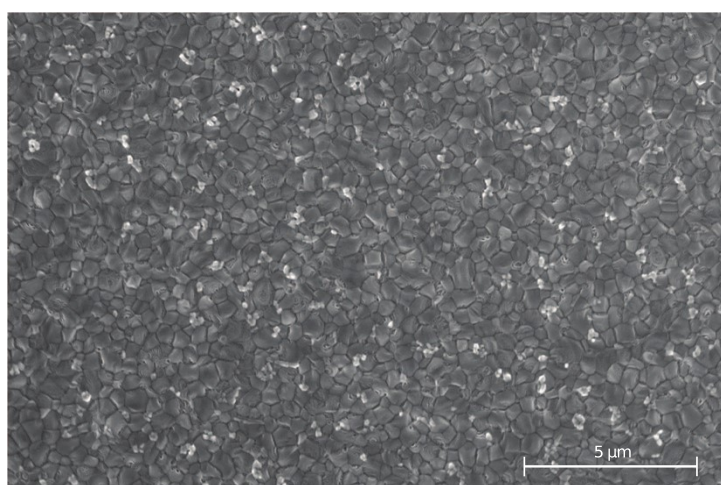
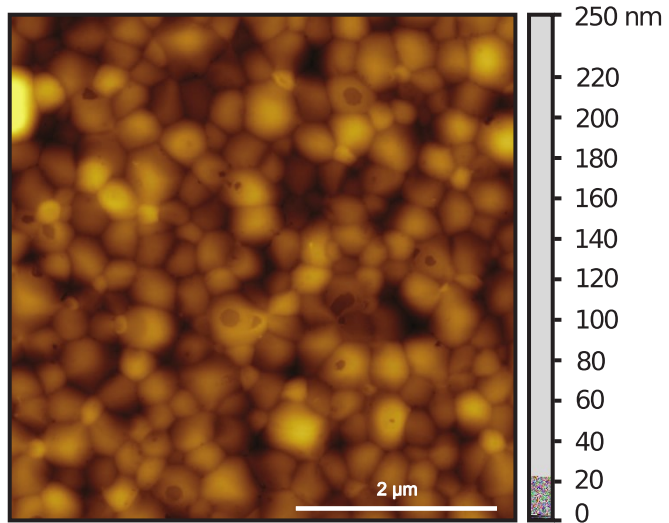
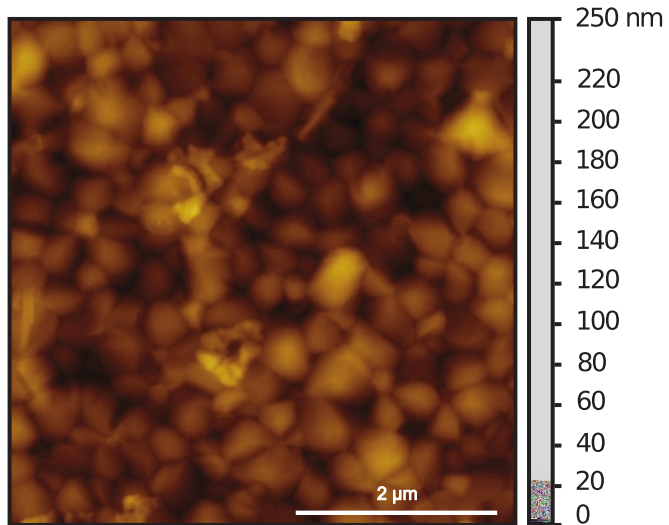


Figure S6. SEM images recorded on the perovskite surface deposited on a) PEDOT: PSS, b) 2PACz, and c) Br-2PACz. Red circles in a) panel highlights the presence of pinholes on the perovskite surface.

(a)



(b)



(c)

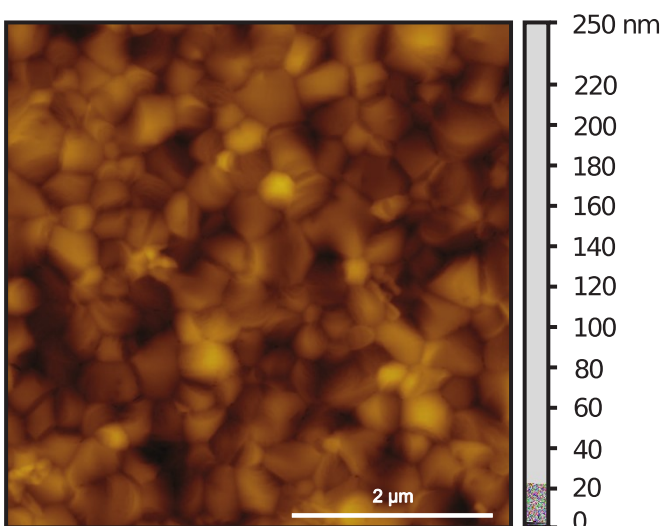


Figure S7. AFM height map for a) ITO/PEDOT/Perovskite, b) ITO/2PACz/Perovskite, and c) ITO/Br-2PACz/Perovskite.

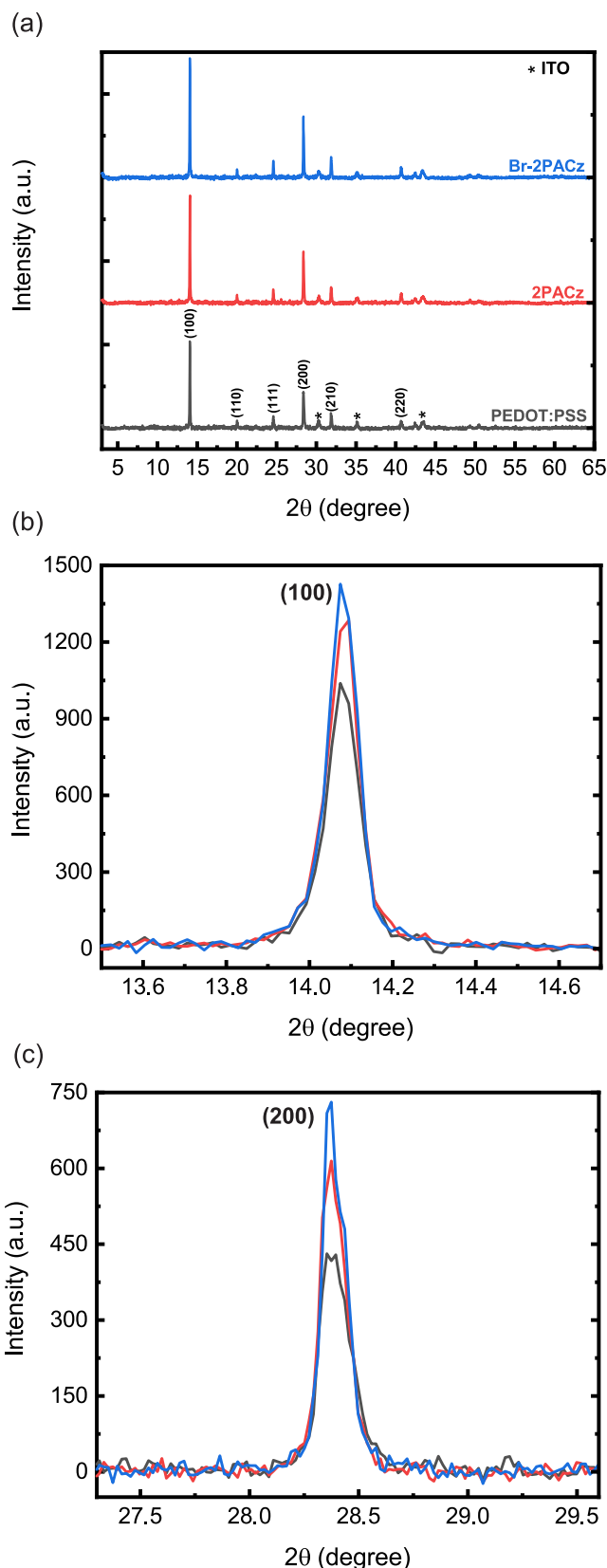


Figure S8. a) XRD patterns for the perovskite material deposited on the different HTLs. Magnification on the b) (100) and c) (200) peaks of the XRD perovskite spectra showed in Figure S8a.

Table S1. Peak position and Full-width half maximum (FWHM) for (100) peak, and the calculated crystallite size and d-spacing for the (100) plane.

	(100) peak position	FWHM	Crystallite size (nm)	d-spacing (Å)
PEDOT:PSS	14.08008	0.09944	79.23604	6.28493
2PACz	14.08045	0.09558	82.43602	6.28477
Br-2PACz	14.08015	0.08878	88.75008	6.28490

Table S2. TRPL decay and average values obtained after fitting the curves showed in Figure 2h.

	$\langle \tau \rangle$ (ns)	τ_1 (ns)	τ_2 (ns)
PEDOT:PSS	44.65	21.67	63.85
Br-2PACz	82.98	28.27	85.11
2PACz	88.23	31.10	119.00

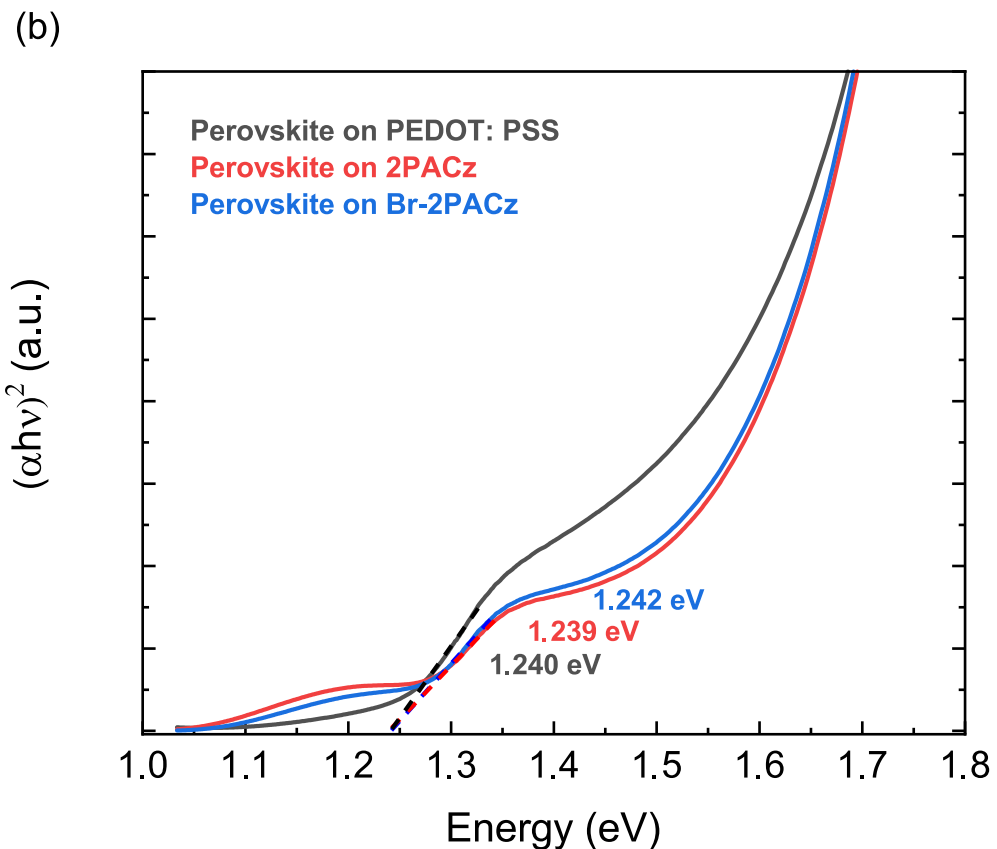
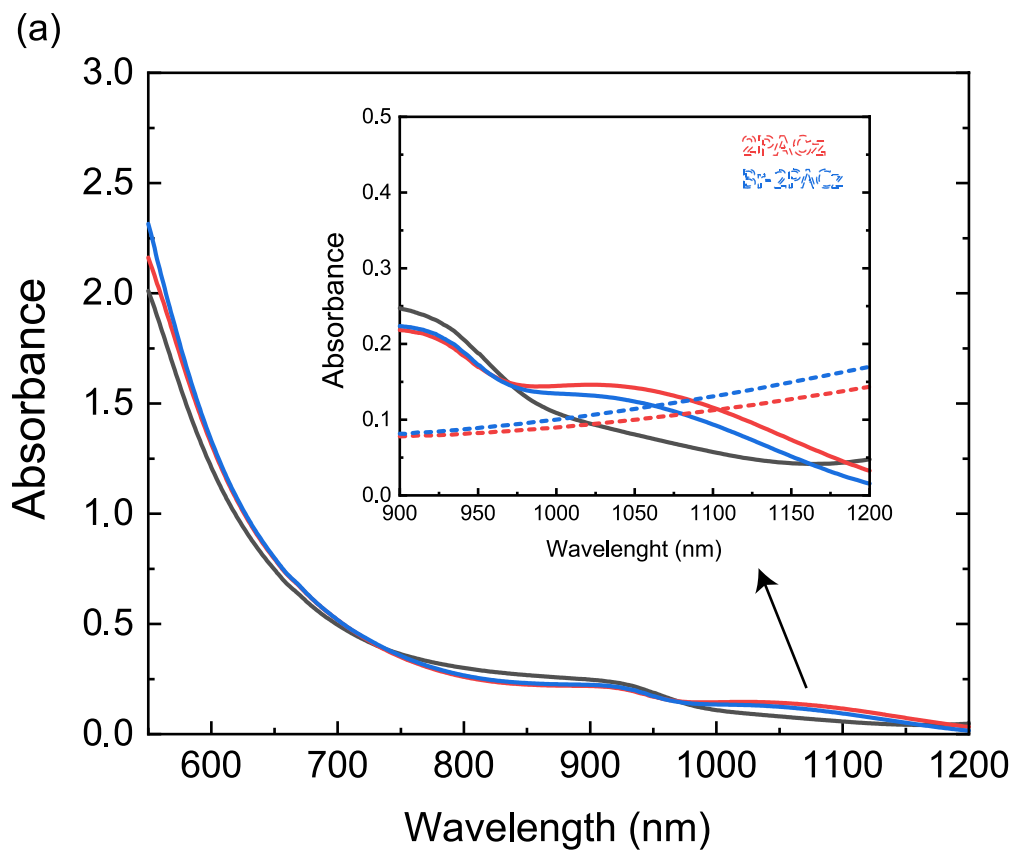


Figure S9. a) Absorbance spectrum and b) Tauc plot for $\text{Cs}_{0.25}\text{FA}_{0.75}\text{Sn}_{0.5}\text{Pb}_{0.5}\text{I}_3$ films deposited on PEDOT: PSS (black line), 2PACz (red line), and Br-2PACz (blue line). Here,

the active layers was deposited with a reduced thickness (340 nm) in order to prevent the photodetectors' saturation.

(a)

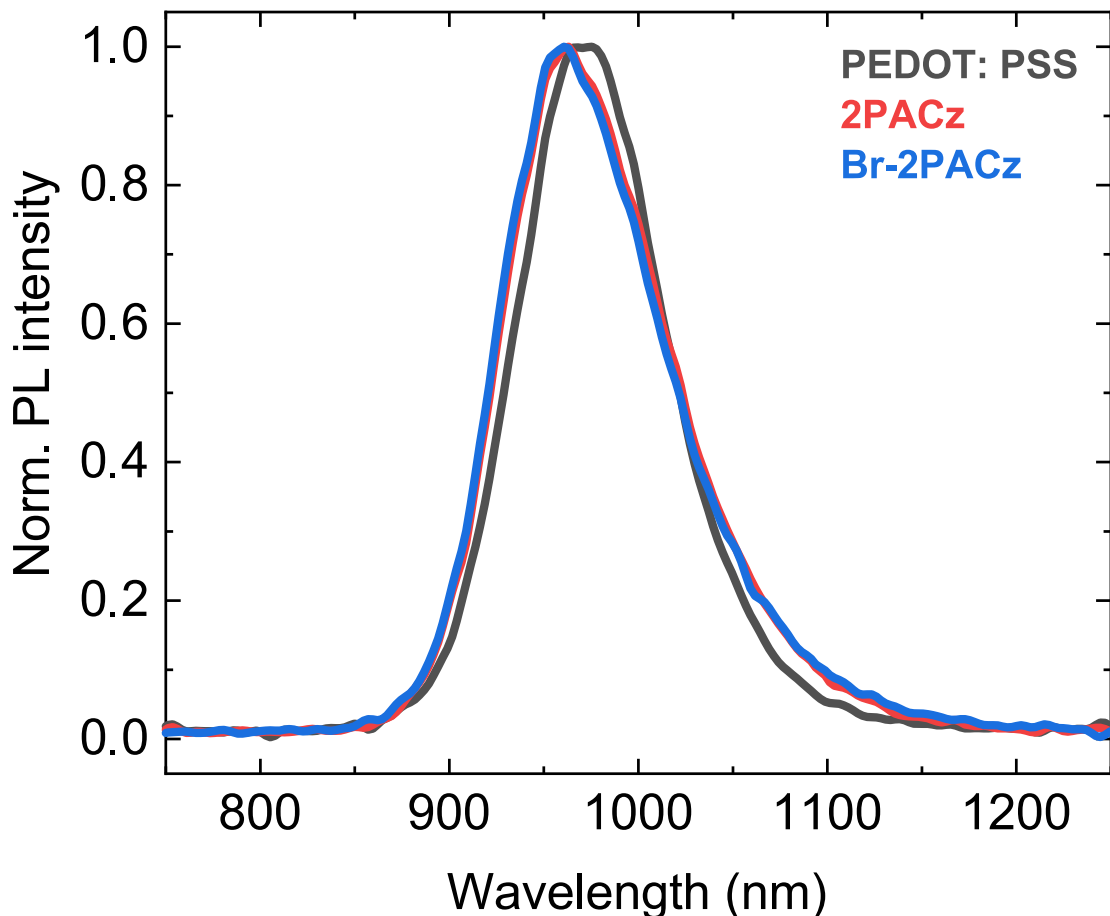
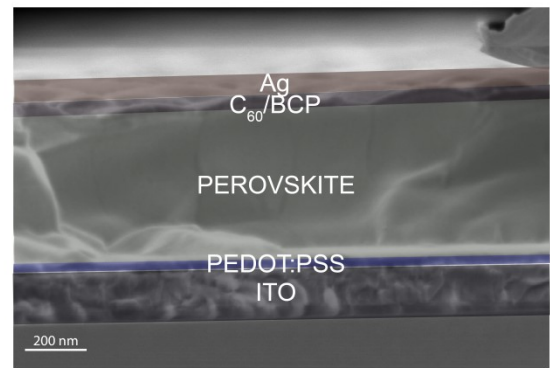
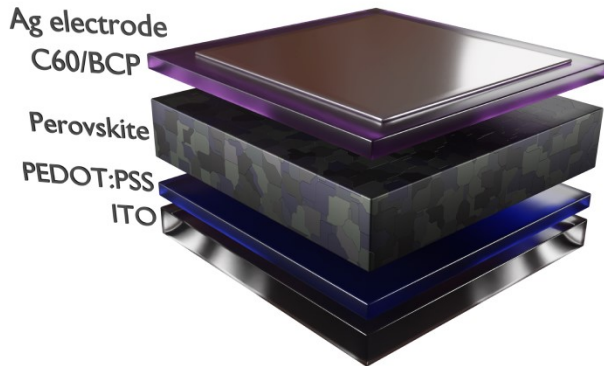


Figure S10. a) Normalized photoluminescence (PL) peaks of the perovskite deposited on PEDOT: PSS (black line), 2PACz (red line), and Br-2PACz (blue line).

Table S3. Average parameter value for the solar cell devices. The values in parenthesis are related to the champion devices.

Device	Jsc (mA cm ⁻²)	Voc (V)	FF	PCE (%)
PEDOT:PSS	29.34 ± 0.70 (30.16)	0.747 ± 0.02 (0.762)	71.35 ± 1.72 (71.05)	15.62 ± 0.57 (16.33)
2PACz	31.33 ± 0.40 (31.11)	0.792 ± 0.01 (0.803)	73.83 ± 0.57 (73.81)	18.13 ± 0.29 (18.44)
Br-2PACz	32.29 ± 0.31 (32.14)	0.793 ± 0.01 (0.810)	75.2 ± 0.82 (74.94)	19.09 ± 0.35 (19.51)

(a)



(b)

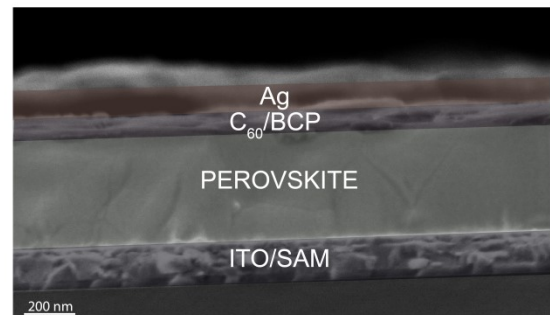
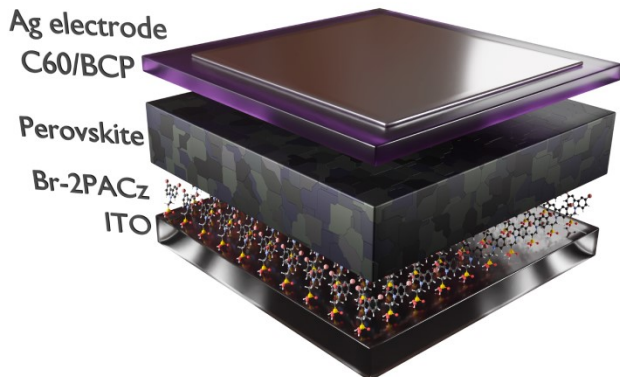


Figure S11. Schematic representation of the device structure on the left, and SEM cross-section image on the right for a) PEDOT: PSS- and b) SAMs- based solar cells.

(a)

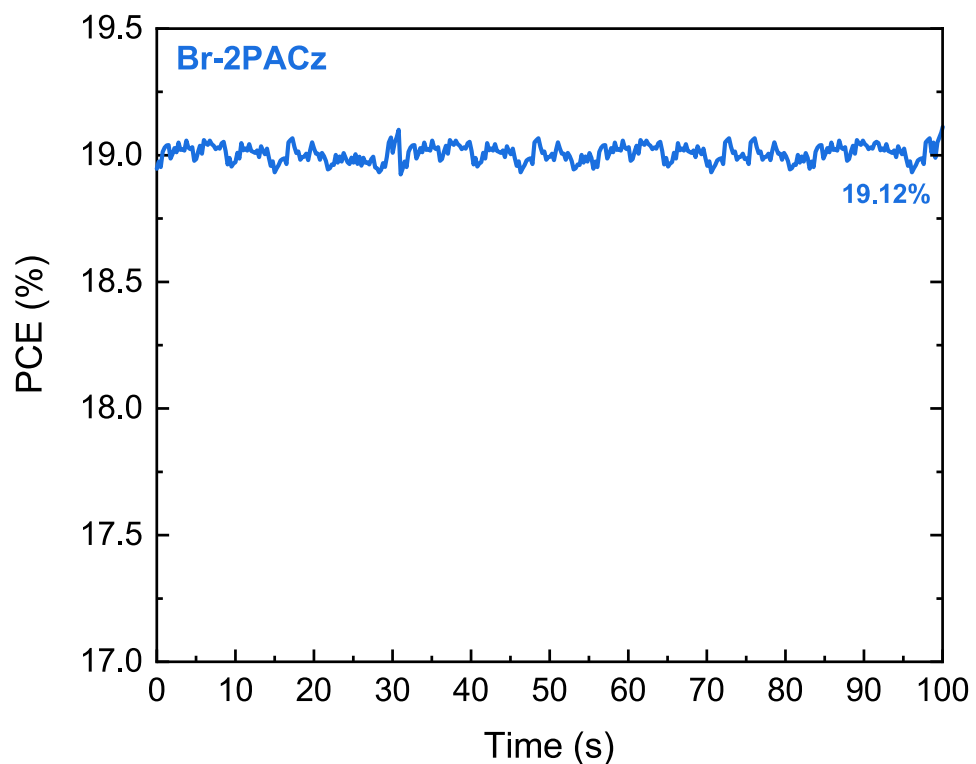


Figure S12. Steady-state power output measured with a constant bias of 0.670 V of the best devices fabricated with Br-2PACz as HTL.

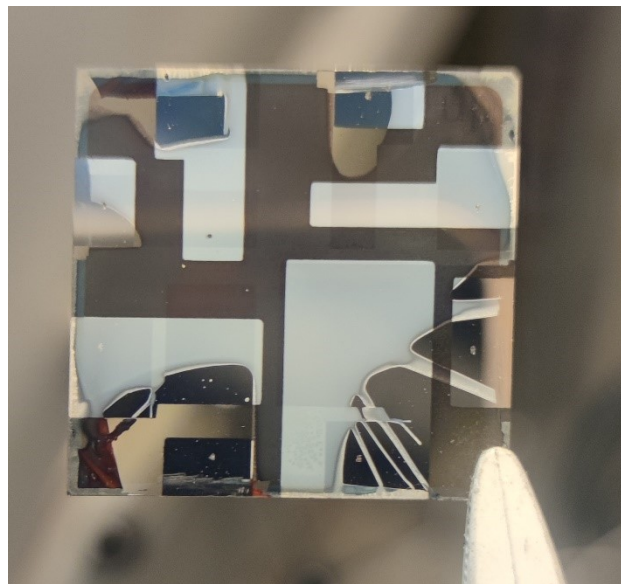


Figure S13. Picture of a solar cells fabricated using Br-2PACz as HTL, without forcing the perovskite solution spreading.

Table S4. Photovoltaic parameters of devices fabricated using 2PACz as HTL without spreading the perovskite solution (reverse measurement).

Device	Jsc (mA/cm ²)	Voc (V)	FF	PCE (%)
1	0.018	4.14	0.24	0.02
2	0.177	13.40	0.27	0.65
3	0.006	1.43	0.00	0.00
4	0.120	9.59	0.25	0.29
5	0.781	31.51	0.76	18.36
6	0.090	17.10	0.25	0.38
7	0.012	2.40	0.13	0.00
8	0.046	4.98	0.25	0.06
9	0.800	30.98	0.73	18.14
10	0.770	31.85	0.72	17.66

(a)

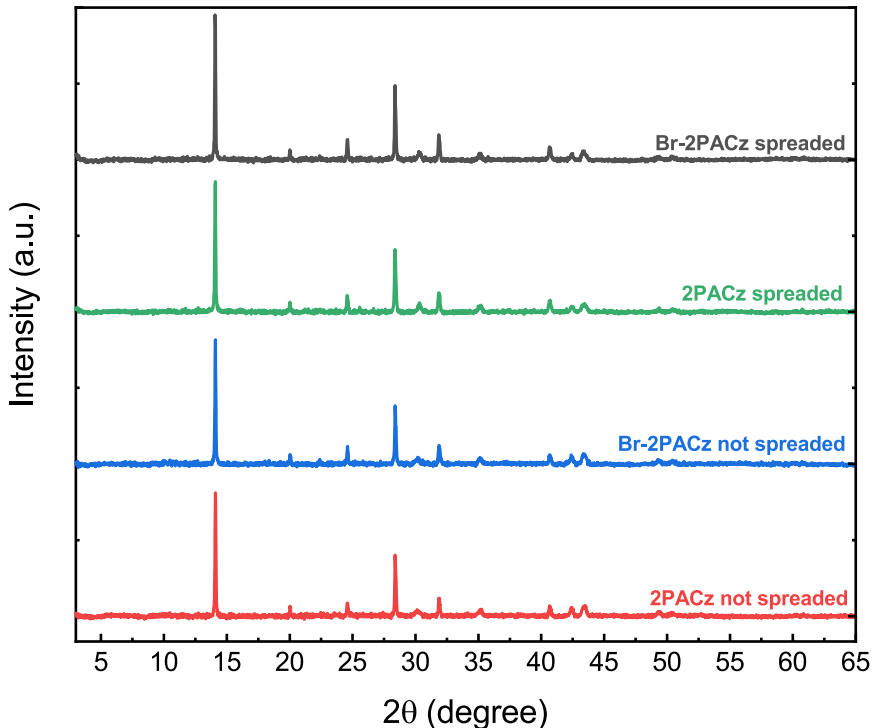


Figure S14. a) XRD spectra for the perovskite deposited on 2PACz and Br-2PACz without forcing the solution spreading (red and blue line, respectively), and for the active layer deposited on 2PACz and Br-2PACz forcing the solution spreading (green and black lines, respectively).

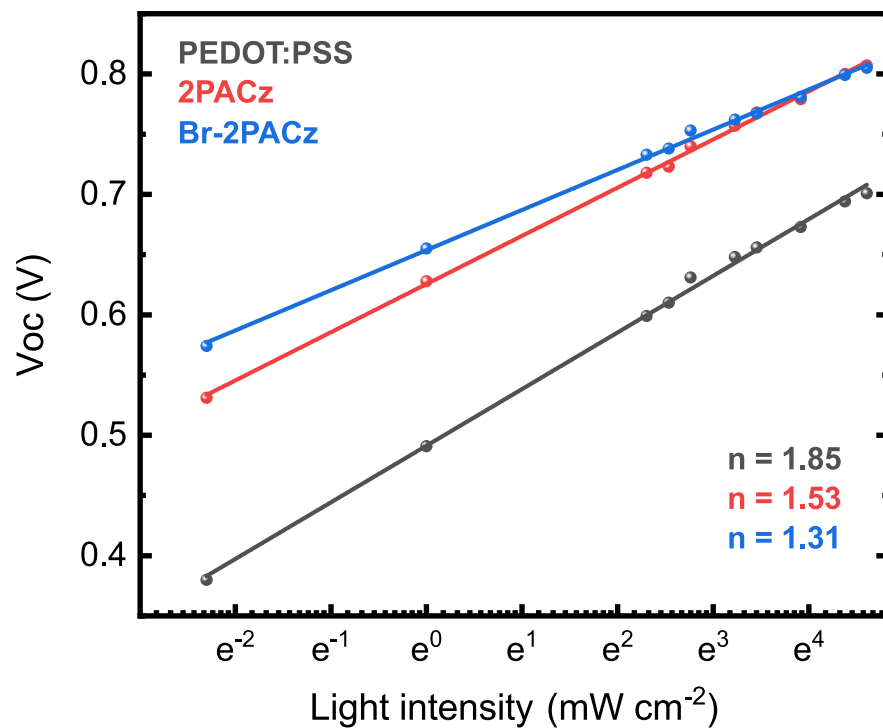
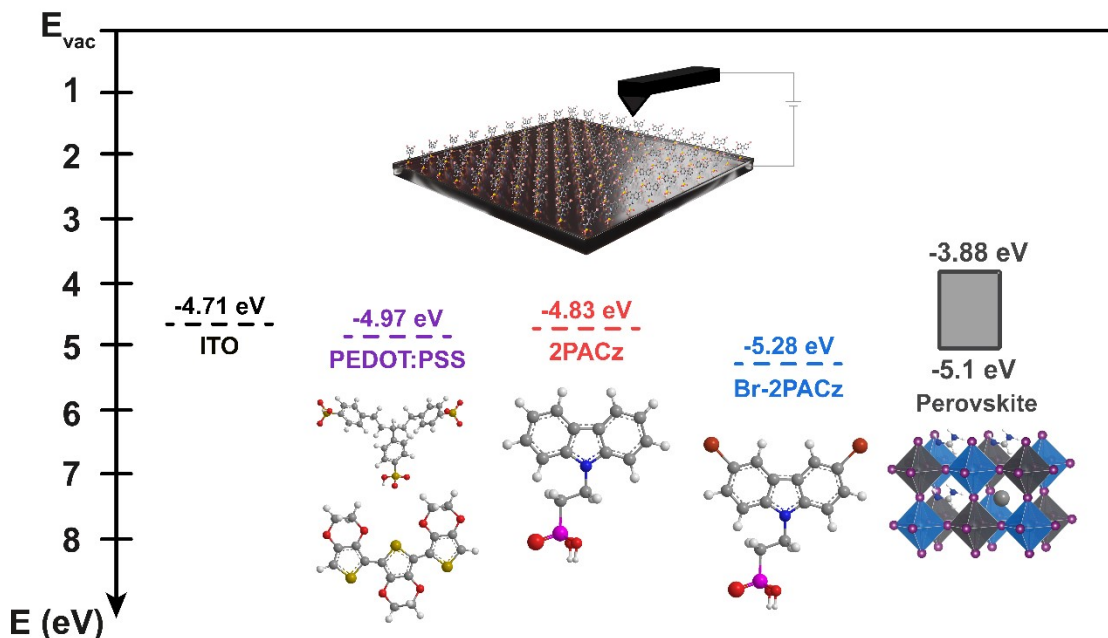
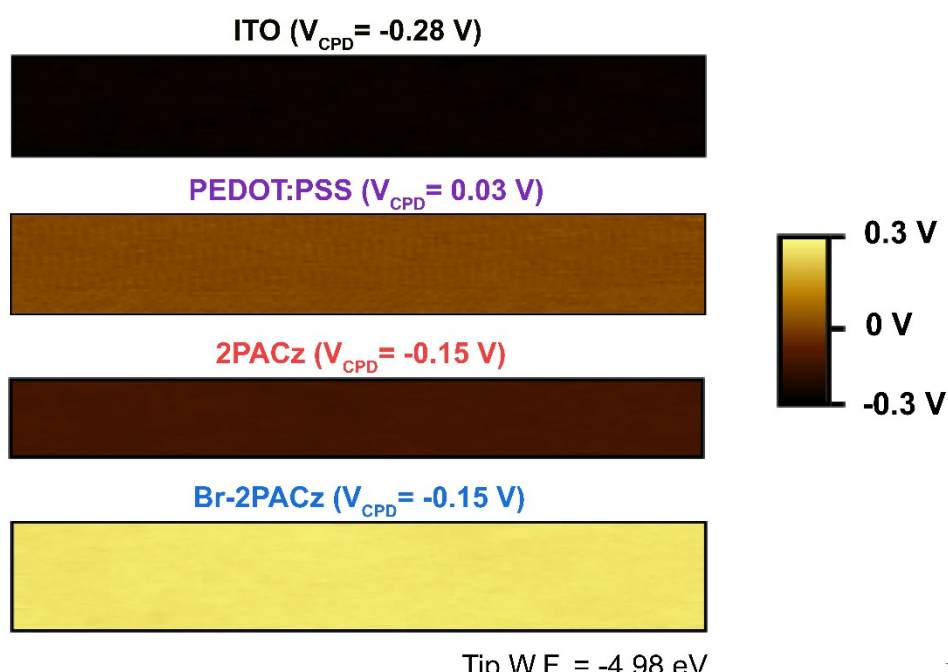


Figure S15. a) V_{oc} versus light intensity plot for solar cells fabricated using PEDOT: PSS (black curve), 2PACz (red curve), and Br-2PACz (blue curve). On the graph are reported the ideality factor for the three different devices.

(a)



(b)

Tip W.F. = -4.98 eV

Figur

e S16. a) Band alignment diagram reporting the WF values for ITO, ITO/PEDOT: PSS, ITO/2PACz, and ITO/Br-2PACz electrodes. In the figure are also reported the valence and conduction band values of the perovskite layer taken from reference ¹. b) KPFM images showing the surface potential profile of ITO, ITO/PEDOT: PSS, ITO/2PACz, and ITO/Br-2PACz electrodes. On the figure, we provided the tip WF measured using a freshly cleaved highly ordered pyrolytic graphite (HOPG) whose work function is 4.6 eV. Finally, in parenthesis it has been reported the contact potential difference for the three different samples.

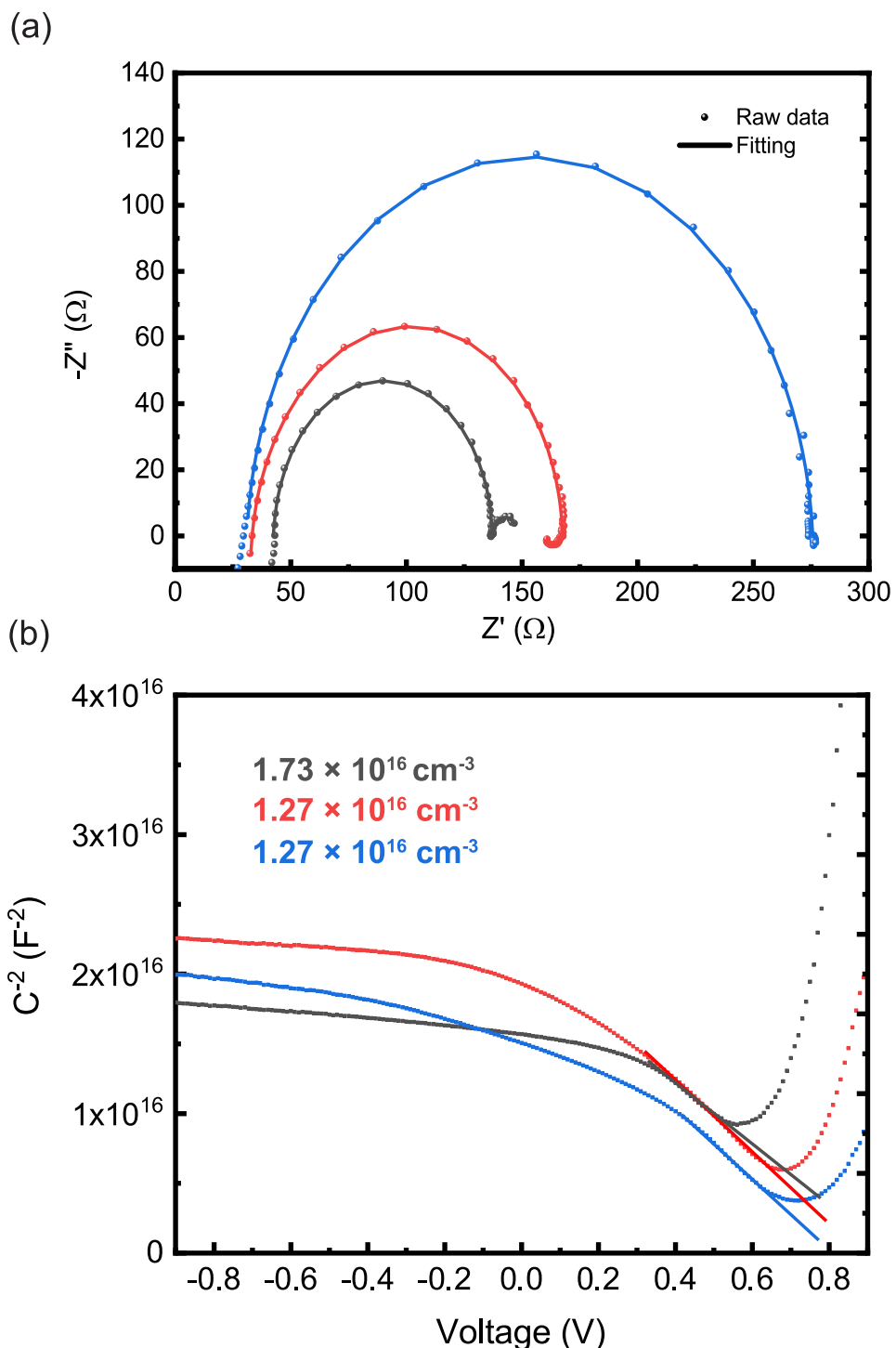


Figure S17. a) Impedance spectroscopy and b) Mott-Schottky analysis for PEDOT: PSS- (black curve), 2PACz- (red curve), and Br-2PACz- (blue curve) based devices.

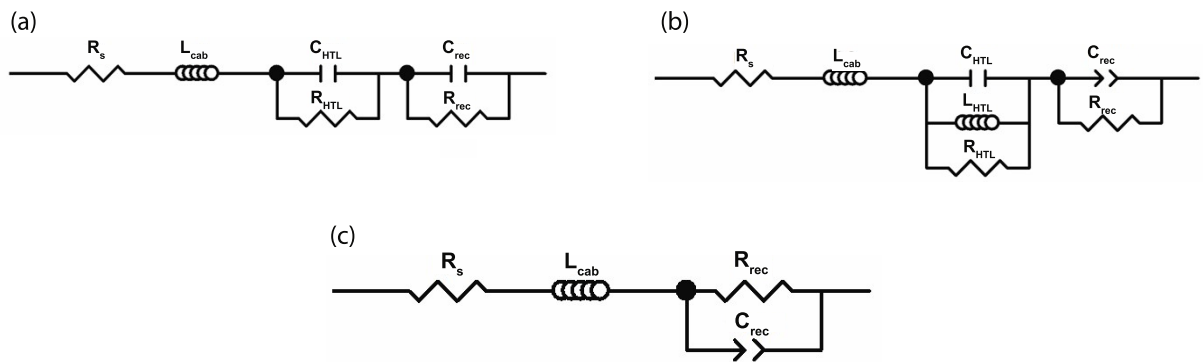


Figure S18. Equivalent circuit used to fit the experimental data for the impedance spectroscopy performed for the solar cells fabricated with a) PEDOT: PSS, b) 2PACz, and c) Br-2PACz as HTL.

Table S5. Series resistance, perovskite/HTL interface resistance, and recombination resistance values for PEDOT: PSS, 2PACz, and Br-2PACz based devices. The values in parenthesis represent the error values for the fitting process.

	PEDOT: PSS	2PACz	Br-2PACz
$R_S (\Omega)$	41.89 (0.16%)	31.58 (0.35%)	30.64 (0.27%)
$R_{HTL} (\Omega)$	11.16 (2.76%)	6.58 (3.12%)	
$R_{rec} (\Omega)$	95.05 (0.1%)	129.3 (0.18%)	245 (0.08%)

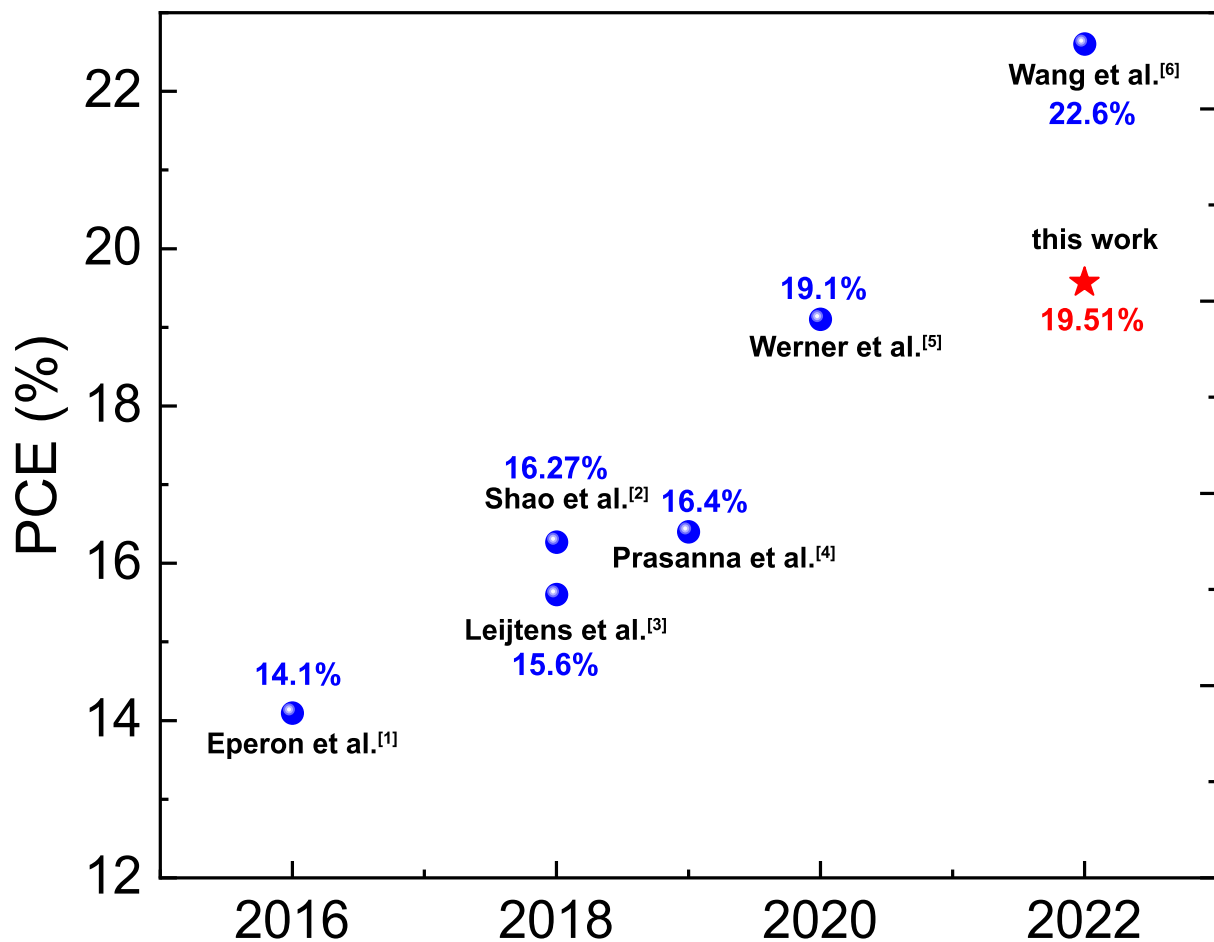


Figure S19. Record chart for the device efficiency of $\text{Cs}_{0.25}\text{FA}_{0.75}\text{Sn}_{0.5}\text{Pb}_{0.5}\text{I}_3$ perovskite solar cells without any anti-reflective coating.¹⁻⁶

- 1 G. E. Eperon, T. Leijtens, K. A. Bush, R. Prasanna, T. Green, J. T. Wang, D. P. Mcmeekin, G. Volonakis, R. L. Milot, R. May, A. Palmstrom, J. Daniel, R. A. Belisle, J. B. Patel, E. S. Parrott, R. J. Sutton, W. Ma, B. Conings, A. Babayigit, H. Boyen, S. Bent, F. Giustino, M. Herz, M. B. Johnston, M. D. Mcgehee and H. J. Snaith, *Science*, 2016, **354**, 861-865.
- 2 S. Shao, Y. Cui, H. Duim, X. Qiu, J. Dong, G. H. Brink, G. Portale, R. C. Chiechi, S. Zhang, J. Hou and M. A. Loi, *Adv. Mater.*, 2018, **30**, 1803703.
- 3 T. Leijtens, R. Prasanna, K. A. Bush, G. E. Eperon, J. A. Raiford, A. Gold-Parker, E. J. Wolf, S. A. Swifter, C. C. Boyd, H. P. Wang, M. F. Toney, S. F. Bent and M. D. McGehee, *Sustain. Energy Fuels*, 2018, **2**, 2450–2459.
- 4 R. Prasanna, T. Leijtens, S. P. Dunfield, J. A. Raiford, E. J. Wolf, S. A. Swifter, J. Werner, G. E. Eperon, C. de Paula, A. F. Palmstrom, C. C. Boyd, M. F. A. M. van Hest, S. F. Bent, G. Teeter, J. J. Berry and M. D. McGehee, *Nat. Energy*, 2019, **4**, 939–947.
- 5 J. Werner, T. Moot, T. A. Gossett, I. E. Gould, A. F. Palmstrom, E. J. Wolf, C. C. Boyd, M. F. A. M. Van Hest, J. M. Luther, J. J. Berry and M. D. McGehee, *ACS Energy Lett.*, 2020, **5**, 1215–1223.
- 6 J. Wang, Z. Yu, D. D. Astridge, Z. Ni, L. Zhao, B. Chen, M. Wang, Y. Zhou, G. Yang, X. Dai, A. Sellinger and J. Huang, *ACS Energy Lett.*, 2022, **7**, 3353–3361.